ACS OMEGA

Open Access

http://pubs.acs.org/journal/acsodf

Article

Application of Low-Salinity Waterflooding in Heavy Oil Sandstone Reservoir: Oil Recovery Efficiency and Mechanistic Study

Xiao Wang,* Xiaoliang Wu, Leiting Shi,* Adil Raad Saadallah Ogaidi, Xuejun Shan, Zhongbin Ye, Guowei Qin, Jingjing Liu, and Bin Wu

Cite This: *ACS Omega* 2024, 9, 30782−30793

Read Online

ACCESS | Metrics & More | Article Recommendations

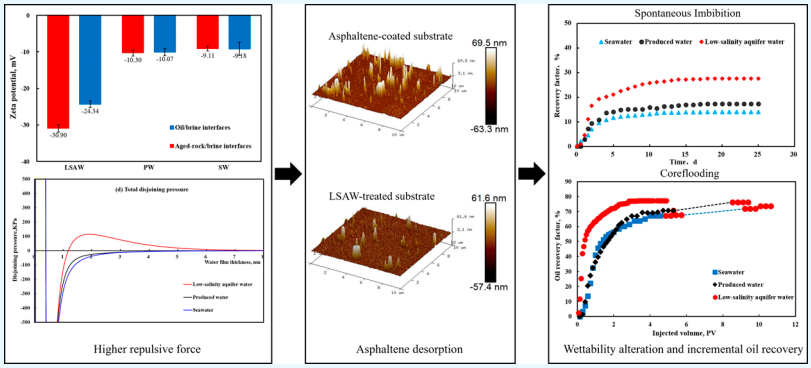

ABSTRACT: Low-salinity water injection (LSWI) is a recently emerged and promising technique to enhance oil recovery. In addition, it is attractive due to its relatively low-cost, environmental friendliness, and sustainability. However, the underlying mechanisms remain unclear, and very limited research has been conducted on heavy oil. To verify the feasibility of injecting a low-salinity aquifer water (LSAW) to improve the oil recovery of our target offshore heavy oil reservoir, first, a series of experiments on the core scale, including coreflooding and spontaneous imbibition experiments, were carried out. Furthermore, atomic force microscopy (AFM), contact angle, zeta potential measurement, as well as disjoining pressure calculations based on the Derjaguin−Landau−Verwey−Overbeek (DLVO) theory were carried out to explore the underlying governing mechanism at the microscopic scale. The secondary oil recovery factors of the coreflood tests are 67.11, 70.55, and 77.18% for seawater (SW), produced water (PW), and LSAW, respectively. The additional oil recoveries by LSAW when injected in tertiary modes are 6.38% after SW injection and 5.68% after PW injection. These results indicate that compared with SW and PW which have high brine salinity, the low-salinity brine from the subsurface aquifer (LSAW) can improve oil recovery in both secondary and tertiary modes. In addition, the oil recovery factors from the spontaneous imbibition tests (27.52% by LSAW, 17.32% by PW, and 14.00% by SW) and the insignificant variation of IFTs among the three brines lead to the anticipation that the LSAW can alter the rock to a more water-wet condition compared with SW and PW, thereby giving rise to a higher oil recovery factor in the coreflooding tests. By using AFM imaging and contact angle tests, we proved that the polar asphaltene could desorb from the rock surface and consequently reduce the water contact angle substantially when subjected to low-salinity brine. Furthermore, the zeta potential and the disjoining pressure results indicate that a more repulsive force was developed between oil and the rock under the low-salinity environment, which thereby promotes asphaltene desorption and consequent wettability alteration. Our work has paved the way to apply LSWI to the offshore heavy oil sandstone reservoir.

1. INTRODUCTION

Heavy oil refers to the oil whose viscosity is in the range of 50 to 50,000 cP and is usually classified as unconventional oil resources. There are vast heavy oil resources worldwide, which account for approximately 15% of the total world oil reserves.[1] As is well-known, heavy oil is rich in polar components, like aromatic oil compounds and organic acids,[2,3] which gives rise to the high viscosity of heavy oil. In addition, the high content of polar components results in the strong adhesion of heavy oil to the rock surface,[4] which alters the rock surface to a less water-wet condition.

Received: April 7, 2024
Revised: June 12, 2024
Accepted: June 14, 2024
Published: July 2, 2024

To improve the heavy oil recovery efficiency, the classical EOR (enhanced oil recovery) methods are generally employed, like the gas injection, chemical injection, as well as thermal methods.[5,6] However, these traditional EOR methods are usually costly.[7] In the last three decades, a relatively new EOR method, i.e., low-salinity water injection (LSWI) with a relatively low salinity, has emerged and attracted attention from both academic and industry fields. LSWI is one promising technique since it is easy to implement. In other words, LSWI is the same as conventional waterflooding, only with adjusted brine salinity. Therefore, compared with the other EOR methods, LSWI has the pronounced advantages of low cost, environmental friendliness, and sustainability. Thereby, LSWI received the award of "Top Ten International Petroleum Science and Technology Progress, 2014".

LSWI as an IOR method was first documented in the late 1950s by Martin;[8] later in the 1960s, Bernard[9] reported an oil recovery increase with LSWI again. However, the research in LSWI did not receive systematic investigation until the early 1990s by the research group of Dr. Morrow at the University of Wyoming. They extensively examined the injection water salinity effect using outcrops and reservoir sandstones. Their experimental work revealed an oil recovery increase when lowering the injection water salinity.[10−12] Later, the research conducted in the other group found that besides the total water salinity, the injection water composition also plays an important role in the oil recovery.[13−15] However, it is worth mentioning that although numerous experiments have shown that low-salinity effect (LSE) in both secondary and tertiary modes, sometimes oil recovery improvements were not observed.[16−18]

Furthermore, based on the experimental observations, various mechanisms to explain the LSE have been proposed by researchers. However, as summarized in Table 1, the underlying mechanisms still remain controversial.

Therefore, by reviewing the oil recovery data and the variously proposed mechanisms, many questions still remain unclear. It is likely that the LSE depends on the specific crude oil−brine−rock (COBR) system. In addition, compared to conventional oil, very limited research was conducted on heavy oil.[37−40] In this study, our target is offshore heavy oil. To test the potential of injecting a low-salinity brine which is available from a subsurface aquifer, first of all, core-scale coreflooding and spontaneous imbibition tests were conducted and compared among three water sources, i.e., seawater, produced water (PW), and low-salinity aquifer water (LSAW). Subsequently, to find the governing mechanisms that affect the waterflood oil recovery, microscale investigations were carried out, including atomic force microscopy (AFM) imaging, contact angle, zeta potential tests, and disjoining pressure calculation.

2. MATERIALS AND METHODS

2.1. Materials. *2.1.1. Crude Oil.* Reservoir crude oil was collected from an offshore heavy oil reservoir (China). Before use in any experiments, the crude oil went through centrifugation (7500 rpm for 5 h) and filtration (11 μm filter paper) to break the emulsion and remove traces of water and solids. The API of the heavy oil is 21.1°. The viscosity−temperature relation was determined using a Brookfield DV-III viscometer. The result is displayed in Figure 1; the heavy oil viscosity at reservoir temperature (65 °C) is 78.3 cP. The saturate−aromatic−resin−asphaltene (SARA) contents of the crude oil were measured by following ASTM D 893-69, and the result is given in Figure 2. The elemental analysis of the crude oil

Table 1. Summary of Some Underlying Mechanisms for LSE

Fine Migration[9,11,19]	This model suggests that LSE arises from the detachment of the oil-attached clays when subject to low-salinity brine, which also promotes the exposure of clean and water-wet rock surfaces.
Contrary Evidence	Numerous studies observed fine migration or permeability reduction without LSE.[20,21] Also, some studies observed LSE but no production of fines or permeability decrease.[14,16,22−26] In addition, the LSE in carbonate proves that LSE is not always associated with fine migration and vice versa.
Multi-ion Exchange (MIE)[23]	This model suggests that the low-salinity brine promotes the adsorption of divalent cations onto clay minerals, exchanging the already adsorbed polar oil components.
Contrary Evidence	According to MIE, clay works as the ion exchanger, indicating that minerals with high cation-exchange-capacity (CEC) are beneficial for LSE. However, kaolinite has been most frequently reported with the occurrence of LSE, even though it possesses a relatively low CEC.[30]
Osmosis[34,35]	This model suggests that during LSWI, clay works as a membrane which separates the low-salinity injection brine and the high-salinity connate water. In this way, it creates an osmotic pressure, which promotes the water drive and mobilizes more oil out of the pore space.
Contrary Evidence	According to this mechanism, the LSE could occur regardless of the oil type, since its function arises from the salinity gradient. However, it has been observed that LSE did not occur with mineral oil.[36]
pH Increase with Surfactant Generation[27]	This model suggests that when crude oil contacts with the low-salinity brine with high pH, saponification occurs between the organic acids in the crude oil and the alkaline water, which behaves similarly to alkaline flooding.
Contrary Evidence	① The high pH (i.e., pH > 9) required for saponification is unlikely available in the actual reservoir due to the existence of CO_2, H_2S, and other pH buffering agents.[28] ② The saponification process requires that the oil should have high acid number (AN). However, LSE has been observed with oils containing little acidic components.[20,28,29]
Double Layer Expansion[25,31]	This model suggests that with LSWI, the electrical double layer expands, leading to the increase of electrostatic repulsion between the adsorbed oil and the mineral surface. When this repulsive force exceeds the binding force, the oil components would desorb from the rock surface and yield more water-wet rock surfaces.
Contrary Evidence	In some mineral surface-scale adhesion tests, it was found that when lowering brine salinity with fixed pH, the adhesion force between the oil and the rock surface increased.[32,33]

https://doi.org/10.1021/acsomega.4c03155
ACS Omega 2024, 9, 30782−30793

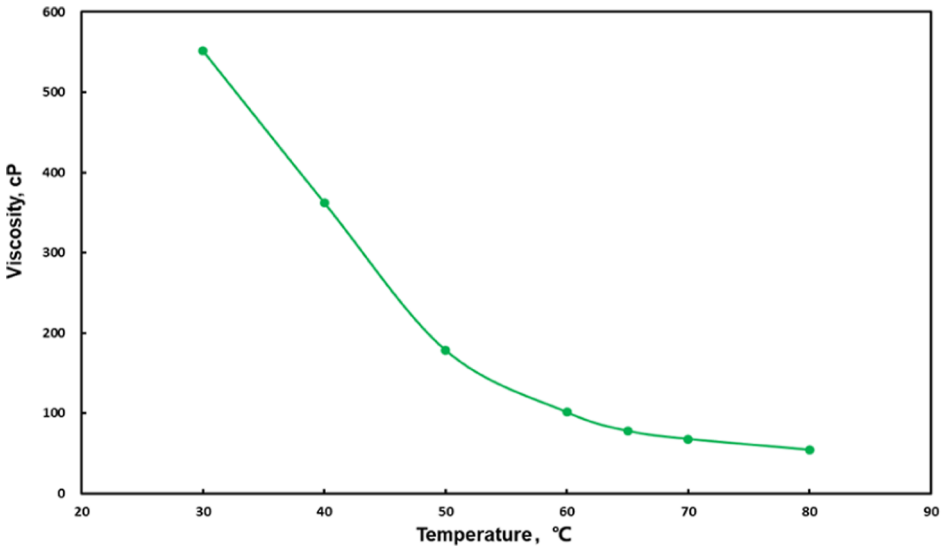

Figure 1. Viscosity−temperature relation of our heavy oil.

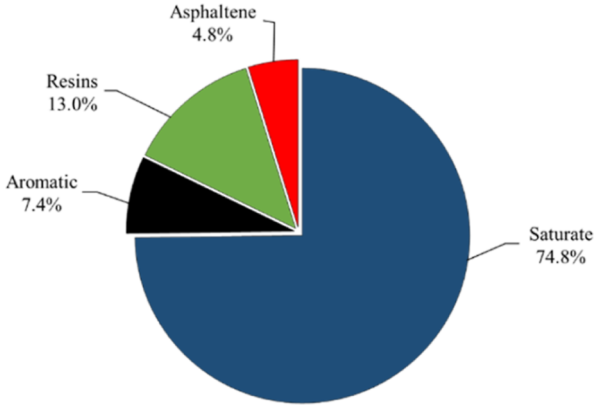

Figure 2. Result of SARA analysis for used crude oil.

was performed using a vario EL III elemental analyzer. The H/C atom ratio was calculated by converting the wt % hydrogen and wt % carbon data to their molar units (as shown in Table 2).

Table 2. Elemental Analysis Results of the Crude Oil

element contents (wt %)					
C	H	O	N	S	H/C atom ratio
82.6	11.2	4.7	0.4	0.5	1.6

2.1.2. Synthetic Brines. Three synthetic brines were prepared and used in this study. The three synthetic brines are as follows: seawater (SW), produced water (PW), and low-salinity aquifer water (LSAW). The ionic composition and basic properties of our synthetic brines are displayed in Table 3. Produced water composition was determined according to the produced water composition from the offshore heavy oil reservoir. Seawater represents a synthetic makeup of the water collected from the nearby sea. Low-salinity aquifer brine represents the brine from a bottom aquifer. All brines were prepared in the laboratory by adding specified amounts of salts in deionized water. All reagents were of analytical grade. The brines were degassed to remove dissolved air prior to each test.

2.1.3. Rock Samples. 2.1.3.1. Reservoir Rocks. Reservoir rocks collected from the oil formation were received. Since the received reservoir rocks were contaminated during coring, they were subject to solvent cleaning using the Dean−Stark setup and subsequently dried before any further tests. Industrial X-ray computed tomography (GE Vtomex) was utilized to observe the microstructures of two representative rock samples. First, 2D projections were collected on both the *Z*-direction and the *R*-direction taken at different angles. Thereafter, a 3D representation of the pore space was reconstructed from a series of 2D projections. As shown in Figure 3, significant intra- and interheterogeneity exist in reservoir rocks. Thereby, in this study, sandpack prepared using drilling cuttings was used in the coreflooding and spontaneous imbibition experiments to have a good quality control. In addition, the micrographs of the reservoir rock were obtained using an FEI (model Quanta 450) scanning electron microscope (SEM) in the secondary electron mode. As shown in Figure 4, the reservoir rock has noticeable interparticle pores, and the pores are connected well. The reservoir rock is mainly made up of medium-size grains (with grain size ∼200 μm), with filling cementation. In addition, the pore surfaces are obviously coated with kaolinite minerals, which occur as face-to-face stacks of plates. Furthermore, the XRD (X-ray diffraction) analysis gives more details about the mineralogical properties of the reservoir rock, as reported in Table 4.

Table 3. Chemical Composition and Properties of the Synthetic Brines Used in This Study

brines	ion concentration (ppm)							TDS (ppm)	ionic strength (M)	pH
	Na^+	K^+	Mg^{2+}	Ca^{2+}	Cl^-	SO_4^{2-}	HCO_3^-			
seawater (SW)	9920	363	1360	486	18,599	2650	159	33,537	0.68	7.6
produced water (PW)	7740	248	480	289	14,760	853	0	24,370	0.45	7.6
low-salinity aquifer water (LSAW)	990	21	35	60	2,041	17	0	3,163	0.06	7.9

https://doi.org/10.1021/acsomega.4c03155
ACS Omega 2024, 9, 30782−30793

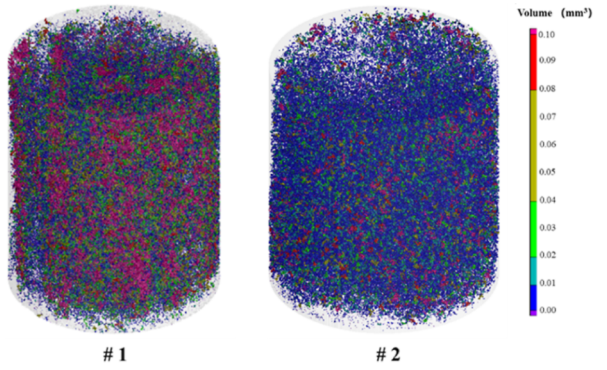

Figure 3. Pore volume distribution of reservoir rocks nos. 1 and 2 obtained by CT scanning.

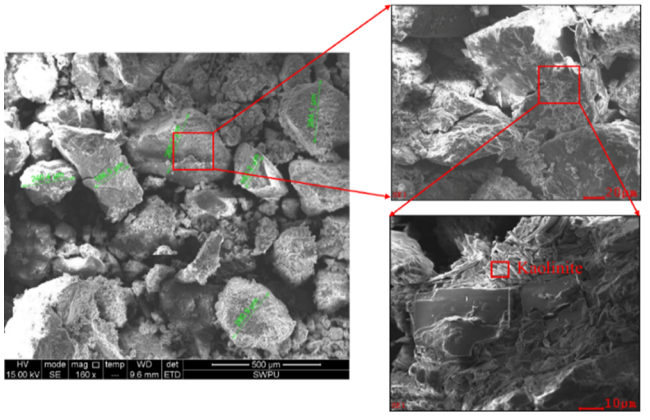

Figure 4. SEM micrograph of the cleaned reservoir rock.

2.1.3.2. Drilling Cuttings. Freshly field-produced drilling cuttings were collected. However, these drilling cuttings were subject to water-based drilling mud contamination. To remove the bentonite coming from the drilling mud while preserving the authigenic clays in the reservoir rocks, the drilling cuttings were cleaned using a 3 wt % KCl solution under agitation. The rationale for this cleaning method is that the external clay from the drilling mud easily floats in the aqueous solution but not for native clays in the cores. Subsequently, methanol was used to clean the KCl. At last, the drilling cuttings were dried in a constant-humidity oven at 65 °C for 24 h. Furthermore, XRD analysis was carried out on the cleaned drilling cuttings, and the results (in Table 4) confirm that cleaned drilling cuttings have close mineral composition with reservoir rocks. Therefore, it is reasonable to use synthetic sandpack prepared with cleaned drilling cuttings to simulate natural reservoir rocks.

2.2. Sandpack Preparation with Drilling Cuttings and Coreflooding. Sandpacks were prepared in this study to conduct the parallel coreflooding experiments. The sandpack core holders were equipped with flow distributors and 200-mesh screens on both ends to prevent fine sands from flowing-out in the experimental process. Cleaned drilling cuttings were packed inside the coreholder using a rod when every layer of sands was added. Desired permeability (close to actual reservoir rock's permeability) was achieved by adjusting the tightness of the sandpack. The dry weight of the sandpack was measured. Subsequently, the pack was vacuumed for 1 h to remove any air, followed by an injection of the formation brine at three different rates to saturate the core sample and obtain the absolute permeability. In addition, the wet weight of the sandpack was measured to calculate the porosity. The basic properties of our prepared sandpacks used for the coreflooding tests are provided in Table 5.

Thereafter, the initial oil saturation was established by injecting oil at three different rates. The oil-saturated sandpack was aged at 65 °C for 2 weeks. Different brines were injected in three parallel tests to displace the oil at the rate of 0.1 cm^3/min, until oil production ceased. The low-salinity aquifer brine was injected to test whether more oil could be produced following the injection of seawater and injection water. All of the coreflooding tests were conducted at the reservoir temperature of 65 °C and a back pressure of atmospheric pressure.

2.3. Artificial Rock Preparation with Drilling Cuttings and Spontaneous Imbibition. Artificial rock samples were prepared using cleaned drilling cuttings to simulate the actual reservoir rocks. Since for the loosely consolidated reservoir rocks, they have been protected with wrapping foils and screens on both ends (as shown in Figure 5a). The artificial rock samples were prepared by packing the cleaned drilling cuttings into a steel tube-like mold. In addition, 200-mesh screens were also installed on both ends of the rock sample (as shown in Figure 5b). Desired permeability, i.e., close to the accrual reservoir rock permeability, was achieved by adjusting the packing pressure.

The dry weight of the rock sample was measured after the packing. Then, they were vacuum-saturated with brine. Porosity was determined from the weight difference. The 100% water-saturated artificial rock sample was mounted into a coreflooding system, and brine permeability was determined by injecting brine at three different rates. Subsequently, oil was injected to establish the initial oil saturation and aged at 65 °C for 2 weeks. The basic properties of the artificial rock samples used in the spontaneous imbibition tests are summarized in Table 6.

The oil-saturated and aged-rock sample was placed in an improved Amott cell. As shown in Figure 6, the traditional Amott cell was improved in two ways: ① the rock sample was suspended in the cell instead of sitting on the bottom, which increases the contact area between the rock sample and the surrounding brine; ② with respect to the issue of oil sticking to the rock surface instead of floating up, the rock sample was fixed to the bottom stopper. In such a way, an external force could be applied to help shake off the adhered oil. The volume of the cumulative displaced oil was recorded at different times. The experiment was conducted at the reservoir temperature of 65 °C.

2.4. Interfacial Tension (IFT) Measurement. The IFT between crude oil and brine was measured using a KRÜSS K100

Table 4. Mineral Composition Results of Rock Samples Used in This Study Obtained by XRD

rock sample	mineral composition (wt %)						
	quartz	feldspar	plagioclase	clay			
				kaolinite	mixed-layer I/S	illite	chlorite
reservoir rock	55.9	15.8	17.9	6.0	2.7	1.4	0.3
drilling cuttings	56.0	11.0	23.9	6.0	1.6	1.1	0.4

https://doi.org/10.1021/acsomega.4c03155
ACS Omega 2024, 9, 30782−30793

Table 5. Basic Properties of the Artificially Prepared Sandpacks Used in the Coreflooding Tests

sandpack ID	diameter (cm)	length (cm)	porosity (%)	brine permeability (mD)	injected brine in secondary mode	injected brine in tertiary mode
DCCF-01	2.6	8.5	31.6	863	SW	LSAW
DCCF-02	2.6	8.4	32.0	850	PW	LSAW
DCCF-03	2.6	8.5	31.3	868	LSAW	LSAW

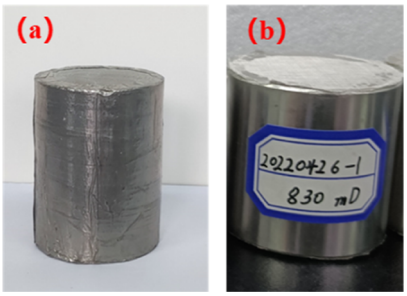

Figure 5. Rock samples: (a) natural reservoir rock and (b) artificially prepared rock sample for the spontaneous imbibition test.

Table 6. Basic Properties of the Artificially Prepared Core Samples Used in the Spontaneous Imbibition Tests

core ID	diameter (cm)	length (cm)	porosity (%)	brine permeability (mD)	surrounding brine
DCIM-01	2.5	4.0	31.9	815	SW
DCIM-02	2.5	4.0	31.5	823	PW
DCIM-03	2.5	4.0	32.4	830	LSAW

Figure 6. Improved Amott cell.

tensiometer at the reservoir temperature of 65 °C. The Du Noüy ring equipped with the tensiometer was initially in the brine phase. Then the ring was pulled, passing the brine−oil interface, after the oil was poured slowly above the brine. In this process, the IFT was measured and recorded.

2.5. Asphaltene-in-Toluene Solution Preparation. First, asphaltenes were extracted from the crude oil using the modified ASTM D 6560 (IP143) standard method.[41] Briefly, *n*-heptane was mixed with the crude oil at a ratio of 30:1 (*n*-heptane/crude oil, mL/g). The mixture was refluxed under stirring for 1 h and left to stand overnight. The mixture was then filtered by using a 0.2 μm filter. The precipitates were collected, and the waxy substances were removed with *n*-heptane using a Soxhlet extractor until the solution became clear. Afterward, toluene was utilized to extract asphaltenes from the residual filtrate. The obtained asphaltenes in a toluene solution were concentrated and dried.

The asphaltene solution (1.0 g/L) was prepared by dissolving the precipitated asphaltene into toluene by overnight mixing. Then, the asphaltene-in-toluene solution was stored in a sealed glass vial wrapped with aluminum foil, preventing exposure to light. Before each use, the solution was sonicated for 5 min and degassed to eliminate possible bubbles.

2.6. Atomic Force Microscopy Imaging. The surface topographies of the glass slides were characterized using AFM (Bruker Instrument, Germany) in the Peakforce tapping mode. Prior to each test, the substrate was cleaned using an ultrasonic device for 30 min in tensioactive solution, then rinsed with 10% nitro-acid, and finally washed with deionized water (DI water). After cleaning and drying, the glass substrates were incubated in formation brine for 1 week. Then, the substrates were removed from the formation brine and allowed to drain but not to dry. To have asphaltene deposition on the glass slides, the substrates were then incubated in asphaltene solution at 65 °C for 2 weeks. The aged substrates were then briefly rinsed with toluene to remove the loosely deposited asphaltenes. Afterward, the slides were placed in various brines at 65 °C for 1 day to simulate the waterflood process. The AFM imaging measurements were performed with a silicon cantilever with a nominal spring constant of 3 N/m at a scan rate of 1.0 Hz. The scanning area is 10 μm × 10 μm. All measurements were performed at 25 °C.

2.7. Contact Angle Measurement. The contact angle tests were conducted on glass slides. The water−air−glass contact angles of variously treated glass slides were measured by using a KRÜSS drop shape analyzer (DSA100, Germany) with deionized water as the probing liquid. The procedures were repeated on six different spots for each sample, and the results were averaged. The contact angle measurement was conducted at ambient pressure and room temperature.

2.8. Zeta Potential Measurement. The zeta potentials of both the solid−brine and oil−brine interfaces were measured by using the Zetasizer Nano (Malvern). The measurement principle is electrophoretic light scattering. In this study, the oil phase used is the asphaltene-in-toluene solution when measuring the zeta potential of the oil−brine interface. The oil−brine emulsions were prepared at a volume ratio of 1:19 and stirred using a magnetic stirring apparatus. To measure the solid−brine interface zeta potential, aged-silica particles (with a size of 325 mesh) were utilized in the experiment. To age the fresh silica particles, the powders were soaked in asphaltene solution for 48 h, after which the suspension was filtered through

https://doi.org/10.1021/acsomega.4c03155
ACS Omega 2024, 9, 30782−30793

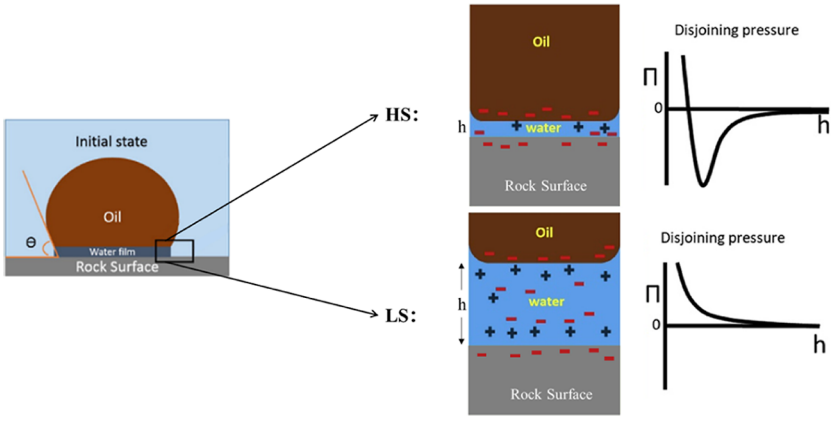

Figure 7. Schematic of the interaction between oil and rock across a thin water film in a COBR system.

0.45 μm filter papers using a vacuum pump. The filtered silica powders were dried at room temperature for 48 h. After that, the aged silica in brine suspensions was prepared by dispersing 1 g of SiO_2 (with the size of 325 mesh) in 200 mL brine and sonicated for 10 min. The average zeta potential was obtained from three measurements at room temperature.

2.9. DLVO Theory and Disjoining Pressure Calculation. The DLVO theory was developed by Derjaguin,[42] Landau,[43] Verwey, and Overbeek.[44] This theory has been applied to the COBR system to describe the interaction between the oil and rock surfaces, which provides insight into the stability of the thin water film. According to this theory, in the COBR system, the main intermolecular forces between two charged interfaces include the van der Waals (vdW) force, electrical double layer force, and structural force. The net force, described by eq 1, is the disjoining pressure. If the disjoining pressure is negative, attractive forces between the oil and rock occur, indicating an unstable water film. On the contrary, a positive disjoining pressure indicates the repulsive interaction between oil and rock and a consequent thick water film, as illustrated in Figure 7.

$$\Pi_t(h) = \Pi_{vdW}(h) + \Pi_{EDL}(h) + \Pi_S(h) \tag{1}$$

where h is the water film thickness; Π_t, Π_{vdW}, Π_{EDL}, and Π_S are the total disjoining pressure, vdW force, electrical double layer force, and structural force, respectively.

2.9.1. vdW Force. The vdW force (Π_{vdW}) is a universal force that exists between any molecules−surfaces and is a function of their distance (h). Generally, the vdW force is attractive, weak, and long-range and comprises orientation force, induction force, and dispersion force. According to Hirasakl's work,[45] $\Pi_{vdW}(h)$ could be calculated by the following formula

$$\Pi_{vdW}(h) = -\frac{A\left(\frac{15.96h}{\lambda_{lw}} + 2\right)}{12\pi h^3\left(1 + \frac{5.32h}{\lambda_{lw}}\right)^2} \tag{2}$$

where h is the water film thickness; A is the Hamaker constant; and λ_{lw} is the London wavelength.

The Hamaker constant depends on the material properties of dielectric constants and refractive indices,[46] which could be calculated by the following formula[47]

$$A = (\sqrt{A_{rock}} - \sqrt{A_{water}})(\sqrt{A_{oil}} - \sqrt{A_{water}}) \tag{3}$$

where subscripts rock, water and rock indicate Hamaker constants for the individual media in vacuum. In this study, the values for A_{rock}, A_{water}, and A_{oil} are adopted as 6.3×10^{-20} J, 3.7×10^{-20} J, and 6.25×10^{-20} J, respectively.[46,48] According to eq 3, the Hamaker constant A is calculated as 0.71×10^{-20} J. The London wavelength λ_{lw} is assumed to be 100 nm in the current study.[13]

2.9.2. Electrical Double-Layer Force. The electrical double-layer force (Π_{EDL}) exists between two charged surfaces due to their surface potentials. In the COBR system, the rock and oil surfaces develop electrical charge through ionization/dissolution of surface groups and adsorption of ions from solution when water is present. The electrical double-layer force between charge oil and rock can be calculated by[49]

$$\Pi_{DLR}(h) = n_b K_B T\left(\frac{2\psi_{r1}\psi_{r2}\cosh(\mathcal{K}h) - \psi_{r1}^2 - \psi_{r2}^2}{(\sinh(\mathcal{K}h))^2}\right) \tag{4}$$

where n_b is the ion density in the bulk solution, given by eq 5; K_B is the Boltzmann constant, 1.38×10^{-23} J/K; T is the absolute temperature in kelvin; ψ_{ri} is the reduced surface potential of the rock−brine and oil−brine interface, given by eq 7; $\mathcal{K}$ is the reciprocal Debye−Huckel double length, given by eq 8.

$$n_b = 2IN_A \tag{5}$$

where I is the ionic strength in the bulk solution, calculated by eq 6; N_A is Avogadro's constant, 6.02×10^{-23} mol^{-1}.

$$I = \frac{1}{2}\sum_i^n C_i Z_i^2 \tag{6}$$

where C_i is the ionic concentration in the bulk solution; Z_i is the ion valence.

$$\psi_{ri} = \frac{e\xi_i}{TK_B} \tag{7}$$

where e is the electron charge, 1.6×10^{-9} C; ξ_i is the surface potential of the rock−brine and oil−brine interface, which is estimated as the zeta potential in this study.

$$\mathcal{K}^{-1} = \sqrt{\frac{\varepsilon_0\varepsilon_r K_B T}{e^2 n_b}} \tag{8}$$

where ε_0 is the vacuum dielectric constant; ε_r is the relative dielectric constant of the aqueous medium.

2.9.3. Structural Force. The structural force (Π_S) is caused by the hydration effect of the aqueous solution, which is valid at a distance less than 5 nm.[50] The structure of water molecules close

https://doi.org/10.1021/acsomega.4c03155
ACS Omega 2024, 9, 30782−30793

to an interface is different from that in the bulk due to the fact that at short distances, the water molecules are ordered in layers. When the two interfaces approach each other, these layers are squeezed, giving rise to the hydration force. The structural force decays exponentially as the water film increases, usually calculated by eq 9.

$$\Pi_s(h) = A_s \exp\left(-\frac{h}{h_s}\right) \quad (9)$$

where A_S is a coefficient and h_S is the characteristic decay length. In this study, $A_S = 1.5 \times 10^{10}$ Pa and $h_S = 0.05$ nm are utilized, as suggested by other work.[51]

3. RESULTS AND DISCUSSION

3.1. Coreflooding Results. With respect to our target offshore oil reservoir, the available water resources could be PW, seawater, and LSAW from a subsurface aquifer. To evaluate their waterflood oil recovery efficiency, three parallel coreflood experiments using three different brines were carried out with sandpacks. In addition, after the injection of PW and seawater, LSAW was injected in tertiary mode. The results are displayed in Figure 8 and Table 7. When comparing the secondary waterflood efficiency, the order is LSAW (77.18%) > PW (70.55%) > seawater (67.11%). Furthermore, the LSAW produces oil at a noticeably higher rate than PW and seawater do, which is especially attractive for offshore oil reservoirs considering the limited lifetime of the platform. The tertiary waterflood results also demonstrate that the LSAW also gives incremental oil recovery.

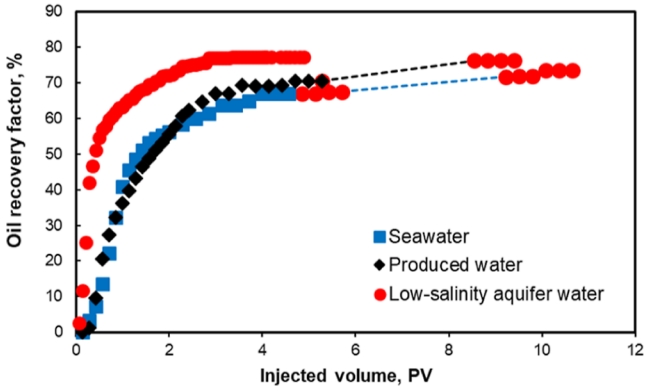

Figure 8. Oil recovery factor obtained from coreflooding tests using sandpacks.

3.2. Spontaneous Imbibition Results. Spontaneous imbibition has been regarded as a reliable method to evaluate the wettability of a porous medium at the core scale. As is well-known, capillary pressure is the only driving force to imbibe the surrounding fluid during the spontaneous imbibition process. Meanwhile, the capillary pressure is highly dependent on the rock wettability. Therefore, it is reasonable to inspect the wettability status by evaluating the amount of oil displaced-out or brine sucked-in.

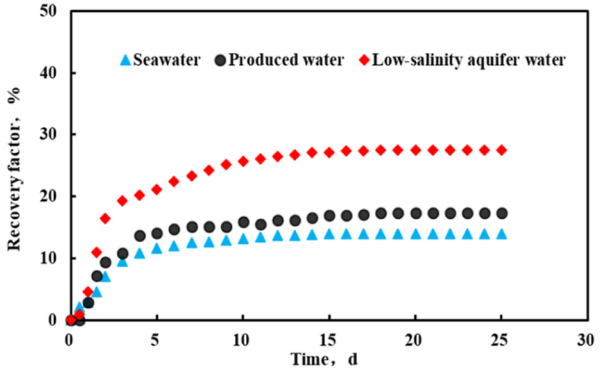

Figure 9. Oil recovery factor obtained from spontaneous tests.

Table 8. Interfacial Tensions (IFTs) between the Three Brines and Crude Oil

brine	seawater	produced water	low-salinity aquifer water
IFT (mN/m)	31.6	31.0	29.9

Table 9. Quantitative Measure of the Roughness and Height of Different Substrates

substrate	bare	asphaltene-aged substrate	after exposure to brines		
			SW	PW	LSAW
RMS (nm)	1.2	9.4	8.8	7.8	6.1
average height (nm)	4.1	37.8	32.9	29.6	18.1

In this study, three parallel tests were conducted to evaluate the oil recovery factors by spontaneous imbibition of three different brines. The results are displayed in Figure 9. As can be seen, for all three cases, the imbibition rates were high at the early stage. After approximately 5 days, the rates started to decline and finally reached zero. In addition, the ultimate oil recovery factors generated by the three different brines are in the order of LSAW (27.52%) > PW (17.32%) > seawater (14.00%), which also indicates the water-wetness in different brines. The IFTs between the three brines and crude oil are collected and are displayed in Table 8. It is evident to see that the brine type has negligible effect on the interfacial tension. Combines with the spontaneous imbibition results, it is reasonable to anticipate that significantly different wetting states are induced by different brines.

3.3. Underlying Mechanisms Investigation: Brine-Dependent Asphaltene Desorption. The above-stated core-scale coreflooding and spontaneous imbibition tests have demonstrated that LSAW has a great potential to reach a high waterflood efficiency compared with PW and seawater, and the wettability alteration plays an essential role in this process. In

Table 7. Summary of the Coreflooding Test Results[a]

sandpack ID	injection water sequence	initial oil saturation (%)	secondary oil RF (%)	additional tertiary oil RF (%)	ultimate oil RF (%)
DCCF-01	SW-LSAW	71.43	67.11	6.38	73.49
DCCF-02	PW-LSAW	72.86	70.55	5.68	76.23
DCCF-03	LSAW	75.00	77.18	N/A	77.18

[a]RF refers to recovery factor.

https://doi.org/10.1021/acsomega.4c03155
ACS Omega 2024, 9, 30782−30793

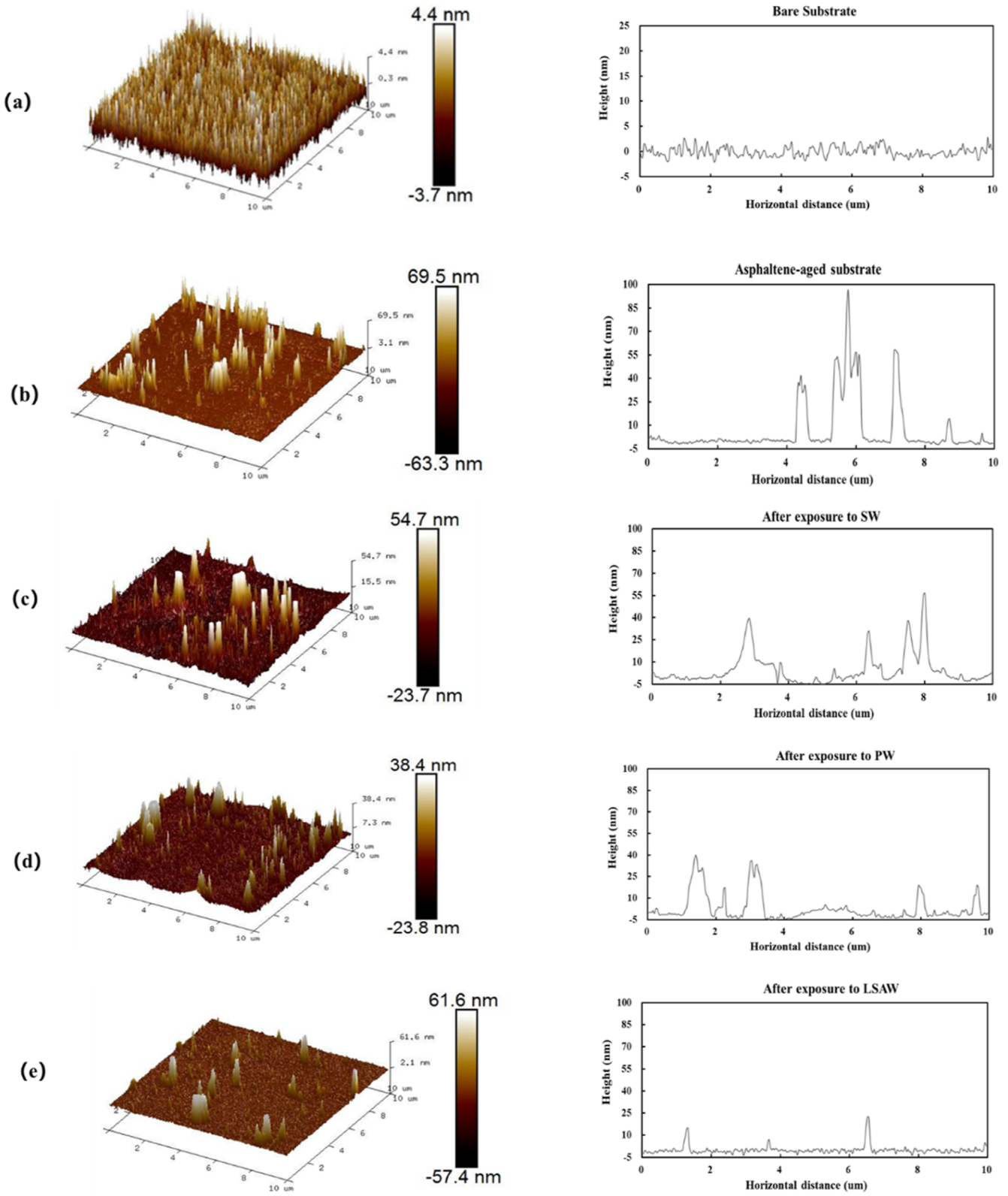

Figure 10. AFM images and height profiles of different substrates: (a) bare substrate, (b) asphaltene-aged substrate, (c) asphaltene-coated substrate after exposure to SW, (d) asphaltene-coated substrate after exposure to PW, and (e) asphaltene-coated substrate after exposure to LSAW.

this section, microscale experimental and theoretical work were carried out to unveil the underlying mechanism of wettability alteration caused by asphaltene desorption.

3.3.1. AFM Imaging of Asphaltene Desorption from the Quartz Substrate. To provide direct evidence of asphaltene desorption extent when exposed to different brines, AFM imaging was utilized to show the asphaltene deposition layer topography on quartz surfaces down to the molecular level. The height distribution of the asphaltene layer was evaluated by section line analysis of AFM topography. The average root

https://doi.org/10.1021/acsomega.4c03155
ACS Omega 2024, 9, 30782−30793

Table 10. Water Contact Angle of the Silicon Substrate before and after Asphaltene Desorption

substrate	bare	asphaltene-aged substrate	after exposure to brines		
			SW	PW	LSAW
contact angle (°)	36.6	95.0	81.4	75.6	67.8

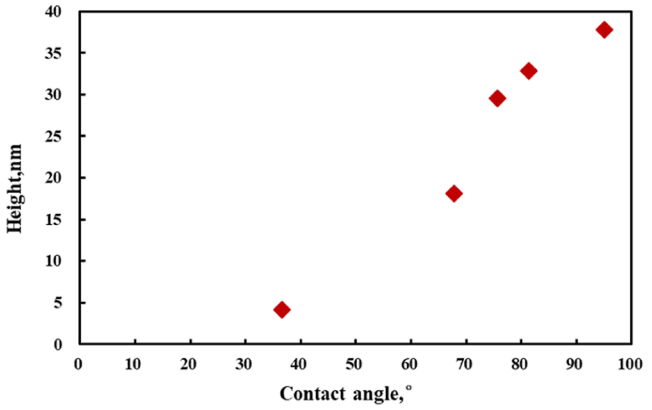

Figure 11. Correlation of asphaltene aggregate height and water contact angle.

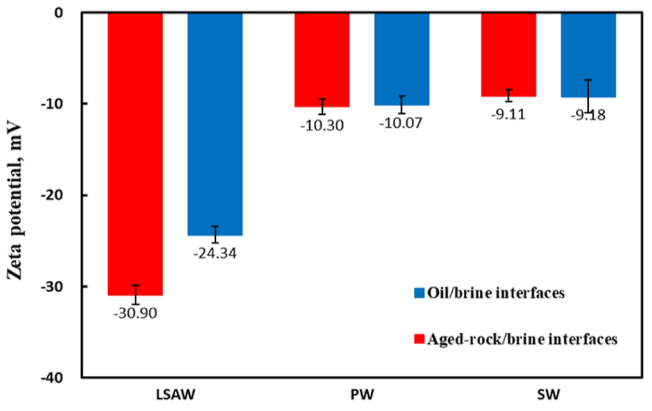

Figure 12. Zeta potential of oil–brine and aged-rock–brine interfaces in different brines.

mean-square (RMS) value (S_q) of the surface roughness was statistically analyzed by the image analysis software. All of the AFM imaging data are summarized in Table 9 and Figure 10.

As shown in Figure 10a, the bare substrate is smooth and homogeneous, with an average RMS roughness (S_q) of 1.58 nm. After two-step aging with formation of brine and asphaltene solution, as shown in Figure 10b, the substrate surface becomes substantially rougher with a roughness (S_q) around 10.07 nm, which is attributed to asphaltene deposition. From Figure 10b, it is easy to see that the asphaltenes are randomly distributed in the form of closely packed nanoaggregates. The average height of these nanoaggregates is 37.8 nm. When the asphaltene-coated surfaces were exposed to various brines, i.e., seawater, PW, and LSAW, as can be observed (Figure 10c–e), the asphaltene-covered fraction of the surface area decreased, thereby expositing the hydrophilic quartz to the sounding brine. In addition, the height of the asphaltene aggregates decreases as well. A closer inspection of Figure 10c–e reveals that the asphaltene-covered surface area and the height of the asphaltene nanoaggregates are in the order of: seawater > PW > LSAW, which indicates high potential for LSAW to desorb the asphaltene.

3.3.2. Contact Angle Results. Contact angle is an easy and direct way to quantify the wettability of a three-phase system. In this study, the asphaltene desorption effect (on rock surface wettability) caused by the surrounding brine variation was investigated by using the water contact angle. The water contact angles were measured on a bare silica substrate, asphaltene-aged silica substrate, and asphaltene-covered substrate after exposure to various brines. As shown in Table 10, the water contact angle of fresh silica was 36.6°, whereas it increased to 95.5° after two-step aging with the formation of brine and asphaltene solution, which indicates asphaltene adsorption on the silica substrate. After exposure to seawater, PW, and LSAW, the water contact angle decreased to 81.4, 75.6, and 67.8°, respectively. This trend illustrates that LSAW is most efficient in asphaltene desorption. Furthermore, the correlation between the height of asphaltene aggregates (Figure 11) confirms that the propensity of asphaltene adhesion on rock surface is directly related to the wettability.

3.3.3.. Zeta-Potential Results and Disjoining Pressure. To further explain asphaltene desorption phenomena and its effect on wettability alteration from the molecular level, zeta potential measurement and subsequent disjoining pressure calculation were conducted, which could explain the brine-dependent interaction force between oil and rock.

As is described in Israelachvili's work,[52] the oil–brine and rock–brine interfaces can become charged through ionization or dissociation of surface groups, or adsorption/binding of ions from bulk solution to the surface. Therefore, the charge gained by the surfaces when water is present is brine-dependent. Usually, the zeta potential is measured in the lab to quantify the amount of surface charge, which is the electrical potential at the shear plane.

In this study, the zeta potentials of both oil–brine and aged-rock–brine interfaces in different brines were measured, and the results are displayed in Figure 12. As can be seen, both the oil–brine and aged-rock–brine interfaces possess a negative zeta potential, which indicates a repulsive force between oil and rock. A further examination of the data reveals that in the low-salinity brine (i.e., LSAW), both interfaces develop the most negative charge, thereby the highest repulsion in between.

To further understand the intermolecular interaction force between oil and the rock surface that promotes asphaltene desorption, the total disjoining pressure and its individual components under different brines were calculated according to the DLVO theory. As shown in Figure 13a–c, in all three brines (i.e., seawater, PW, and LSAW), the vdW forces are all attractive; the structural forces are repulsive and significantly contribute to the disjoining pressure when the water film thickness is less than 0.5 nm; in addition, the electrical double-layer forces are repulsive as well ascribing to the fact that the oil–brine and rock–brine interfaces bear the same charge. When comparing the total disjoining pressure as shown in Figure 13d, the force shifts from attractive to repulsive as the brine ionic strength decreases from 0.68 M (seawater) and 0.45 M (PW) to 0.06 M (LSAW). This phenomenon indicates that when using LSAW, the interaction force between oil and rock is repulsive, which thereby promotes asphaltene desorption.

4. CONCLUSIONS

To find out the potential and the underlying mechanisms of available LSAW on enhancing oil recovery for an offshore heavy

https://doi.org/10.1021/acsomega.4c03155
ACS Omega 2024, 9, 30782–30793

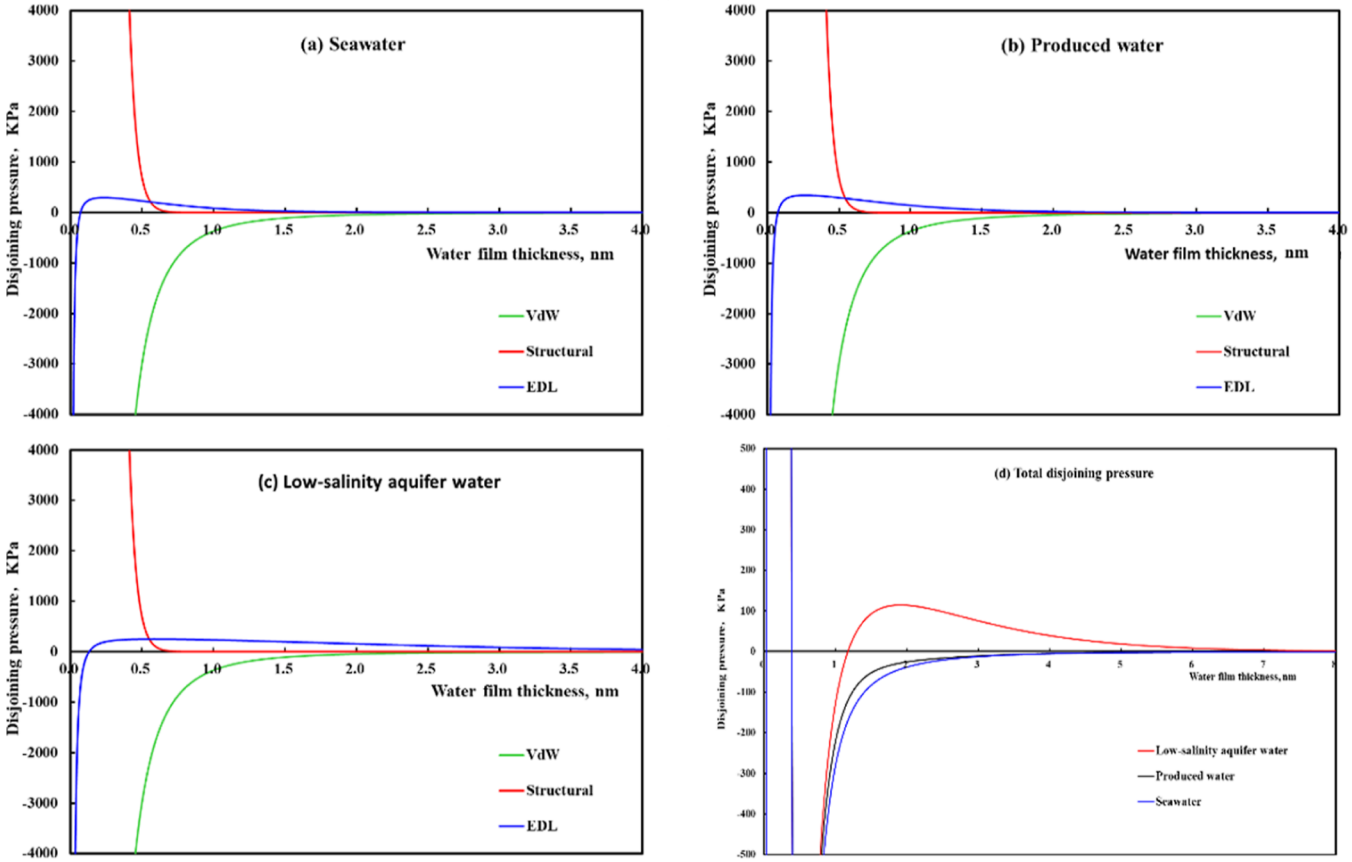

Figure 13. Total disjoining pressure and its individual components as a function of the water film thickness under different brines.

oil, a series of experimental and theoretical works were carried out in this work. The following critical points are pinpointed:

① For our target offshore heavy oil reservoir, the available water sources to inject include the seawater, PW, and LSAW. By conducting coreflooding tests using sandpacks prepared with drilling cuttings, it shows that seawater and PW produce similar ultimate oil recovery, i.e., 67.11% by SW and 70.55% by PW. In comparison, the LSAW results in faster production rate and higher ultimate oil recovery factor (77.18%). In addition, when the LSAW is injected in tertiary mode, more oil is also produced (additional 6.38% and 5.68% OOIP after SW and PW injection, respectively), which indicates that LSAW works in both secondary and tertiary modes.

② The spontaneous imbibition results (27.52, 17.32, and 14.00% for LSAW, PW, and SW, respectively) combined with the insignificantly variant IFTs confirm that LSAW leads to a more water-wet condition compared with SW and PW. To find out the underlying mechanism of wettability alteration, AFM imaging and contact angle tests were carried out and proved that the polar asphaltene desorption is the reason to make the rock surface more water-wet.

③ Furthermore, to explain the asphaltene desorption rational, zeta potential test and disjoining pressure calculation were performed based on the DLVO theory. The results indicate that when subjected to LSAW, a pronounced repulsive force was developed between the oil and rock surface, which thereby promoted the asphaltene desorption.

AUTHOR INFORMATION

Corresponding Authors

Xiao Wang − *State Key Laboratory of Oil & Gas Reservoir and Exploitation, Southwest Petroleum University, Chengdu 610500, China; School of Petroleum and Natural Gas Engineering, Southwest Petroleum University, Chengdu 610500, China;* orcid.org/0000-0002-6666-2205; Email: wx228223@163.com

Leiting Shi − *State Key Laboratory of Oil & Gas Reservoir and Exploitation, Southwest Petroleum University, Chengdu 610500, China; School of Petroleum and Natural Gas Engineering, Southwest Petroleum University, Chengdu 610500, China;* orcid.org/0000-0003-3813-7873; Email: slting@swpu.edu.cn

Authors

Xiaoliang Wu − *School of Petroleum and Natural Gas Engineering, Southwest Petroleum University, Chengdu 610500, China*

Adil Raad Saadallah Ogaidi − *School of Petroleum and Natural Gas Engineering, Southwest Petroleum University, Chengdu 610500, China; EBS Petroleum Company Limited, Baghdad 10011, Iraq*

Xuejun Shan − *China Sinopec International Petroleum Exploration and Production Corporation, Beijing 100029, China*

Zhongbin Ye − *State Key Laboratory of Oil & Gas Reservoir and Exploitation, Southwest Petroleum University, Chengdu 610500, China; Chengdu Technological University, Chengdu 611730, China*

https://doi.org/10.1021/acsomega.4c03155
ACS Omega 2024, 9, 30782−30793

Guowei Qin − *State Key Laboratory of Oil & Gas Reservoir and Exploitation, Southwest Petroleum University, Chengdu 610500, China; College of Petroleum Engineering, Xi'an Shiyou University, Xi'an 710065, China*
Jingjing Liu − *School of Petroleum and Natural Gas Engineering, Southwest Petroleum University, Chengdu 610500, China*
Bin Wu − *School of Petroleum and Natural Gas Engineering, Southwest Petroleum University, Chengdu 610500, China*

Complete contact information is available at:
https://pubs.acs.org/10.1021/acsomega.4c03155

Notes

The authors declare no competing financial interest.

■ ACKNOWLEDGMENTS

We greatly appreciate the financial support from the National Natural Science Foundation of China (grant numbers 52104040 and 52174027), Sichuan Science & Technology Foundation (2023NSFSC0936 and 2023YFH0005), as well as State Key Laboratory of Oil and Gas Reservoir Geology and Exploitation (Southwest Petroleum University, PLN2022-13).

■ REFERENCES

(1) Faergestad, I. *Defining Series: Heavy Oil*; Schlumberger, 2016. https://www.slb.com (accessed March 21, 2024).
(2) Cagna, A.; Esposito, G.; Quinquis, A.-S.; Langevin, D. On the reversibility of asphaltene adsorption at oil-water interfaces. *Colloids Surf., A* **2018**, *548*, 46−53.
(3) Yuan, J.; Elektorowicz, M.; Chen, Z.; Segun, G. A.; Vakili, M.; Zhong, L.; Wang, B.; Zhu, J.; Wu, Y. Simulation and computer modeling of asphaltene in different solvents on oil-water interfaces using a molecular dynamic methodology. *J. Mol. Graphics Modell.* **2019**, *93*, 107450.
(4) Barron, M. G.; Conmy, R. N.; Holder, E. L.; Meyer, P.; Wilson, G. J.; Principe, V. E.; Willming, M. M. Toxicity of Cold Lake Blend and Western Canadian Select dilbits to standard aquatic test species. *Chemosphere* **2018**, *191*, 1−6.
(5) Yang, H.; Lv, Z.; Zhang, M.; Jiang, J.; Xu, B.; Shen, J.; Jiang, H.; Kang, W. A novel active amphiphilic polymer for enhancing heavy oil recovery: Synthesis, characterization and mechanism. *J. Mol. Liq.* **2023**, *391*, 123210.
(6) Yang, H.; Lv, Z.; Wang, L.; Feng, C.; Wang, J.; Xu, Z.; Huang, Y.; Li, Z.; Kang, W. Stability mechanism of controlled acid-resistant hydrophobic polymer nanospheres on CO_2 foam. *Fuel* **2023**, *346*, 128332.
(7) Alomair, O.; Al-Dousari, M.; Azubuike, N.; Garrouch, A. A. Evaluation of the impact of low-salinity water on wettability alteration and oil recovery in Berea sandstones. *Fuel* **2023**, *337*, 127151.
(8) Martin, J. C. The effects of clay on the displacement of heavy oil by water. In *Proceedings of SPE Venezuelan Annual Meeting*, Caracas, Venezuela, October 14−16, 1959; Society of Petroleum Engineers, 1959.
(9) Bernard, G. G. Effect of floodwater salinity on recovery of oil from cores containing clays. In *Proceedings of SPE California Regional Meeting*, Los Angeles, California, October 26−27, 1967; Society of Petroleum Engineers, 1967.
(10) Jadhunandan, P.; Morrow, N. R. Effect of wettability on waterflood recovery for crude-oil/brine/rock systems. *SPE Reservoir Eng.* **1995**, *10* (01), 40−46.
(11) Tang, G.-Q.; Morrow, N. R. Influence of brine composition and fines migration on crude oil/brine/rock interactions and oil recovery. *J. Pet. Sci. Eng.* **1999**, *24* (2−4), 99−111.
(12) Yildiz, H.; Valat, M.; Morrow, N. Effect of brine composition on wettability and oil recovery of a Prudhoe Bay crude oil. *J. Can. Pet. Technol.* **1999**, *38* (01), PETSOC-99-01-02.
(13) Austad, T.; RezaeiDoust, A.; Puntervold, T. Chemical mechanism of low salinity water flooding in sandstone reservoirs. In *Proceedings of SPE Improved Oil Recovery Conference*, Tulsa, Oklahoma, April 24−28, 2010; Society of Petroleum Engineers, 2010.
(14) RezaeiDoust, A.; Puntervold, T.; Austad, T. Chemical verification of the EOR mechanism by using low saline/smart water in sandstone. *Energy Fuels* **2011**, *25* (5), 2151−2162.
(15) Torrijos, I. P.; Puntervold, T.; Strand, S.; Rezaeidoust, A. Optimizing the low salinity water for EOR effects in sandstone reservoirs-composition vs salinity. In *78th EAGE Conference and Exhibition 2016*; European Association of Geoscientists & Engineers, 2016; Vol. *2016*, pp 1−5.
(16) Rivet, S. M.; Lake, L. W.; Pope, G. A. A coreflood investigation of low-salinity enhanced oil recovery. In *Proceedings of SPE Annual Technical Conference and Exhibition*, Florence, Italy, September 19−22, 2010; Society of Petroleum Engineers, 2010.
(17) Sharma, M.; Filoco, P. Effect of brine salinity and crude-oil properties on oil recovery and residual saturations. *SPE J.* **2000**, *5* (03), 293−300.
(18) Skrettingland, K.; Holt, T.; Tweheyo, M. T.; Skjevrak, I. Snorre low-salinity-water injection—coreflooding experiments and single-well field pilot. *SPE Reservoir Eval. Eng.* **2011**, *14* (02), 182−192.
(19) Lever, A.; Dawe, R. A. Water-sensitivity and migration of fines in the hopeman sandstone. *J. Pet. Geol.* **1984**, *7* (1), 97−107.
(20) Boussour, S.; Cissokho, M.; Cordier, P.; Bertin, H.; Hamon, G. Oil recovery by low salinity brine injection: Laboratory results on outcrop and reservoir cores. In *Proceedings of SPE Annual Technical Conference and Exhibition*, New Orleans, Louisiana, October 4−7, 2009; Society of Petroleum Engineers, 2009.
(21) Cissokho, M.; Ahmadi-Senichault, A.; Bertin, H.; Omari, A.; Hamon, G. Some Investigations on the role of microparticles on the low salinity process. In *26 International Symposium of the Society of Core Analysts*; Society of Core Analysis, 2012; p 12.
(22) Alotaibi, M. B.; Azmy, R.; Nasr-El-Din, H. A. A comprehensive EOR study using low salinity water in sandstone reservoirs. In *Proceedings of SPE Improved Oil Recovery Symposium*, Tulsa, Oklahoma, April 24−28, 2010; Society of Petroleum Engineers, 2010.
(23) Lager, A.; Webb, K. J.; Black, C.; Singleton, M.; Sorbie, K. S. Low salinity oil recovery-an experimental investigation1. *Petrophysics* **2008**, *49* (01), SPWLA-2008-v49n1a2.
(24) Lager, A.; Webb, K. J.; Collins, I. R.; Richmond, D. M. LoSal enhanced oil recovery: evidence of enhanced oil recovery at the reservoir scale. In *Proceedings of SPE Improved Oil Recovery Symposium*, Tulsa, Oklahoma, April 20−23, 2008; Society of Petroleum Engineers, 2008.
(25) Ligthelm, D. J.; Gronsveld, J.; Hofman, J.; Brussee, N.; Marcelis, F.; Van der Linde, H. Novel waterflooding strategy by manipulation of injection brine composition. In *Proceedings of SPE Europec featured at EAGE Conference and Exhibition*, Amsterdam, The Netherlands, June 8−11, 2009; Society of Petroleum Engineers, 2009.
(26) Zhang, Y.; Xie, X.; Morrow, N. R. Waterflood performance by injection of brine with different salinity for reservoir cores. In *Proceedings of SPE Annual Technical Conference and Exhibition*, Anaheim, California, November 11−14, 2007; Society of Petroleum Engineers, 2007.
(27) McGuire, P.; Chatham, J.; Paskvan, F.; Sommer, D.; Carini, F. Low salinity oil recovery: An exciting new EOR opportunity for Alaska's North Slope. In *Proceedings of SPE Western Regional Meeting*, Irvine, California, March 30−April 1, 2005; Society of Petroleum Engineers, 2005.
(28) Loahardjo, N.; Xie, X.; Yin, P.; Morrow, N. R. Low salinity waterflooding of a reservoir rock. In *International Symposium of the Society of Core Analyst, Sca2007-29*, 2007.
(29) Pu, H.; Xie, X.; Yin, P.; Morrow, N. R. Low salinity waterflooding and mineral dissolution. In *Proceedings of SPE Annual Technical Conference and Exhibition*, Florence, Italy, September 19−22, 2010; Society of Petroleum Engineers, 2010.
(30) Seccombe, J. C.; Lager, A.; Webb, K.; Jerauld, G.; Fueg, E. Improving Wateflood Recovery: LoSal EOR Field Evaluation. In

Proceedings of SPE Improved Oil Recovery Symposium, Tulsa, Oklahoma, April 20−23, 2008; Society of Petroleum Engineers, 2008.
(31) Hilner, E.; Andersson, M. P.; Hassenkam, T.; Matthiesen, J.; Salino, P.; Stipp, S. L. S. The effect of ionic strength on oil adhesion in sandstone-the search for the low salinity mechanism. *Sci. Rep.* **2015**, *5* (1), 9933.
(32) Lebedeva, E. V.; Fogden, A. Adhesion of oil to kaolinite in water. *Environ. Sci. Technol.* **2010**, *44* (24), 9470−9475.
(33) Lebedeva, E. V.; Fogden, A.; Senden, T. J.; Knackstedt, M. A. *Kaolinite Wettability—The Effect of Salinity, pH and Calcium*; Society of Core Analysts, 2010.
(34) Pollen, E. N.; Berg, C. F. Experimental investigation of osmosis as a mechanism for low-salinity EOR. In *Proceedings of SPE Abu Dhabi International Petroleum Exhibition and Conference*, Abu Dhabi, UAE, November 12−15, 2018; Society of Petroleum Engineers, 2018.
(35) Sandengen, K.; Kristoffersen, A.; Melhuus, K.; Jøsang, L. O. Osmosis as mechanism for low-salinity enhanced oil recovery. *SPE J.* **2016**, *21* (04), 1227−1235.
(36) Rivet, S. M. Coreflooding oil displacements with low salinity brine. Ph.D. Thesis, University of Texas, Austin, USA, 2009.
(37) Babakhani Dehkordi, P.; Razavirad, F.; Shahrabadi, A. Pore-scale displacement of heavy crude oil during low salinity water flooding. *Transp. Porous Media* **2022**, *145* (1), 73−101.
(38) Bhicajee, P.; Romero-Zerón, L. Effect of different low salinity flooding schemes and the addition of alkali on the performance of low-salinity waterflooding during the recovery of heavy oil from unconsolidated sandstone. *Fuel* **2021**, *289*, 119981.
(39) Sánchez-Rodríguez, J.; Gachuz-Muro, H.; Sohrabi, M. Application of low salinity water injection in heavy oil carbonate reservoirs. In *Proceedings of SPE Europec featured at EAGE Conference and Exhibition*, Madrid, Spain, June 1−4, 2015; Society of Petroleum Engineers, 2015.
(40) Tangparitkul, S.; Hodges, C. S.; Ballard, D. A.; Niu, Z.; Pradilla, D.; Charpentier, T. V.; Xu, Z.; Harbottle, D. Dewetting dynamics of heavy crude oil droplet in low-salinity fluids at elevated pressures and temperatures. *J. Colloid Interface Sci.* **2021**, *596*, 420−430.
(41) ASTM International. *Standard Test Method for Determination of Asphaltenes (Heptane Insolubles) in Crude Petroleum and Petroleum Products; ASTM D 6560-22*, 2022.
(42) Derjaguin, B. Theory of particle interaction in presence of double electrical layers and aggregation stability of lyophobic colloids in dispersion systems. *Issue Acad. Sci. USSR, Ser. Chem.* **1937**, *5*, 1153−1164.
(43) Derjaguin, B.; Landau, L. Theory of the stability of strongly charged lyophobic sols and of the adhesion of strongly charged particles in solutions of electrolytes. *Prog. Surf. Sci.* **1993**, *43* (1−4), 30−59.
(44) Verwey, E. J. W.; Overbeek, J. T. G. Theory of the Stability of Lyophobic Colloids. *J. Phys. Chem.* **1947**, *51* (3), 631−636.
(45) Hirasakl, G. Wettability: fundamentals and surface forces. *SPE Form. Eval.* **1991**, *6* (02), 217−226.
(46) Israelachvili, J. N. *Intermolecular and Surface Forces*; Academic Press, 2011.
(47) Awolayo, A. N.; Sarma, H. K.; Nghiem, L. X. Modeling the characteristic thermodynamic interplay between potential determining ions during brine-dependent recovery process in carbonate rocks. *Fuel* **2018**, *224*, 701−717.
(48) Gupta, V.; Miller, J. D. Surface force measurements at the basal planes of ordered kaolinite particles. *J. Colloid Interface Sci.* **2010**, *344* (2), 362−371.
(49) Gregory, J. Interaction of unequal double layers at constant charge. *J. Colloid Interface Sci.* **1975**, *51* (1), 44−51.
(50) Liang, Y.; Hilal, N.; Langston, P.; Starov, V. Interaction forces between colloidal particles in liquid: Theory and experiment. *Adv. Colloid Interface Sci.* **2007**, *134−135*, 151−166.
(51) Morrow, N. R. *Interfacial Phenomena in Petroleum Recovery*; CRC Press, 1990.
(52) Israelachvili, J. N. Van der Waals forces between particles and surfaces. In *Intermolecular and Surface Forces*, 2011; pp 253−289.

https://doi.org/10.1021/acsomega.4c03155
ACS Omega 2024, 9, 30782−30793